Arterial spin labeling versus ^{18}F-FDG-PET to identify mild cognitive impairment

Sudipto Dolui[a,1], Zhengjun Li[a,1], Ilya M. Nasrallah[a], John A. Detre[a,b], David A. Wolk[b,*]

[a] Department of Radiology, University of Pennsylvania, Philadelphia, PA, United States
[b] Department of Neurology, University of Pennsylvania, Philadelphia, PA, United States

ABSTRACT

Neurodegenerative biomarkers support diagnosis and measurement of disease progression in the Alzheimer's disease (AD) continuum. ^{18}F-Fluorodeoxyglucose Positron Emission Tomography (^{18}F-FDG-PET), which measures glucose metabolism, is one of the most commonly used biomarkers of neurodegeneration, but is expensive and requires exposure to ionizing radiation. Arterial Spin Labeled (ASL) perfusion Magnetic Resonance Imaging (MRI) provides non invasive quantification of cerebral blood flow (CBF), which is believed to be tightly coupled to glucose metabolism. Here we aimed to compare the performances of ASL derived CBF and ^{18}F-FDG-PET derived standardized uptake value ratio (SUVR) in discriminating patients with mild cognitive impairment (MCI) from older Controls. 2D pseudo continuous ASL and ^{18}F-FDG-PET data with adequate scan quality from 50 MCI study participants (age=73.0 ± 7.0 years, 16 female) and 35 older controls (age=70.2 ± 6.9 years, 20 female), acquired in close temporal proximity, usually on the same day, were considered for this study. We assessed Control-patient group differences both at voxel level and within a priori regions of interest (ROIs). We also compared their area under receiver operating characteristic curves (AUC) with mean CBF or SUVR in a priori selected posterior cingulate cortex (PCC). CBF and ^{18}F-FDG-PET showed abnormalities in similar areas, particularly in medial temporoparietal regions, consistent with the typically observed pattern of prodromal AD. The hypoperfusion pattern with relative CBF (obtained by normalizing voxel CBF values with mean CBF in putamen) was more localized than with absolute CBF. Pearson's correlation coefficients between the T-scores corresponding to the group-differences obtained with ^{18}F-FDG-PET SUVR and absolute and relative ASL CBF were 0.46 and 0.43 ($p < 0.001$), respectively. ROI analyses were also consistent, with the strongest differences observed in PCC ($p < 0.01$). ^{18}F-FDG-PET SUVR, absolute and relative CBF in the PCC ROI demonstrated moderate and similar discriminatory power in predicting MCI status with AUC of 0.71 ± 0.12, 0.77 ± 0.12 and 0.74 ± 0.13, respectively. In conclusion, ASL CBF may be a reasonable, less expensive and safer substitute for ^{18}F-FDG-PET in clinical research.

1. Introduction

The recent framework for a biomarker definition of Alzheimer's Disease (AD) reflects an increased emphasis on linking the disease to its biological substrate rather than clinical syndrome (Jack et al., 2018; 2016). This classification system defines individuals based on the presence of cerebral amyloid ("A"), neurofibrillary tau-based pathology ("T"), and neurodegeneration ("N"). While "N" is less specific to the molecular pathology that defines AD, the presence of both A and T (Wirth et al., 2013), it is critical for staging disease severity, prognostication of clinical endpoints, and disease monitoring.

[18]F-Fluorodeoxyglucose Positron Emission Tomography (^{18}F-FDG-PET) is the most mature functional biomarker of neurodegeneration (Herholz et al., 2002; Jack et al., 2013; Landau et al., 2011; Mosconi et al., 2009, 2008). It provides a measure of glucose metabolism and is particularly appealing as it is sensitive to neuronal death and alterations of synaptic activity that are considered to reflect AD pathology (Selkoe, 2002). Indeed, a number of studies have demonstrated the sensitivity and predictive value of ^{18}F-FDG-PET measures in preclinical and prodromal stages of AD, termed Mild Cognitive Impairment (MCI) (Chetelat et al., 2003; Herholz et al., 2011; Landau et al., 2011; 2010; Mosconi et al., 2008).

Measures of cerebral blood flow (CBF) are also thought to reflect synaptic activity based on the tight coupling between synaptic activity

and glucose metabolism and between glucose metabolism and CBF (Chen et al., 2011; Raichle, 1998). Arterial Spin Labeled (ASL) perfusion MRI (Alsop et al., 2015; Detre et al., 1992) provides noninvasive quantification of CBF using magnetically labeled blood as an endogenous flow tracer. ASL-MRI has been extensively validated with other established modalities for measuring CBF (Ewing et al., 2005; Heijtel et al., 2014; Koziak et al., 2008; Warmuth et al., 2007; Ye et al., 2000) and has several advantages over ^{18}F-FDG-PET in that it does not require exposure to ionizing radiation, is less expensive, and can be acquired as part of routine MRI, which is almost universally obtained in patients with suspected neurodegenerative conditions.

We previously demonstrated significant overlap between areas of hypoperfusion measured with ASL-MRI and areas of hypometabolism measured by ^{18}F-FDG-PET acquired on the same day in mild-to-moderate AD patients in whom these functional changes are more severe and easier to detect than at earlier stages (Chen et al., 2011; Musiek et al., 2012). The current study aimed to extend the findings to patients with MCI, a clinical diagnosis enriched in patients with prodromal AD. Compared to the previous studies comparing ASL and 18F-FDG-PET in MCI patients (Dolui et al., 2017; Riederer et al., 2018; Tosun et al., 2016), this study includes a larger sample size and/or superior ASL methodology. The current work also leverages recent advances in the signal processing of 2D ASL-MRI data (Dolui et al., 2016a; 2016b).

2. Methods

2.1. Study participants

MRI and ^{18}F-FDG-PET/CT data acquired from 56 MCI patients and 36 older controls, participating in the Penn Memory Center (PMC) cohort, were considered for this study. Data of the MCI patients were collected in parallel with the control subjects. Clinical diagnosis of MCI followed National Institute for Aging – Alzheimer's Association (NIA-AA) core clinical criteria (Albert et al., 2011; Petersen, 2004) and was arrived at by consensus meeting attended by neurologists, psychiatrists, radiologists and neuropsychologists based on medical and neurological examinations, psychometric assessments and imaging (Dolui et al., 2017; Xie et al., 2016). Study inclusion criteria were age 50–85 years, more than 7 years of education, and spoken English. Exclusion criteria included history of clinical stroke, traumatic brain injury, or any other disease or medical/psychiatric condition felt to impact neuropsychological performance. The human subjects' research in this study was performed in compliance with the Code of Ethics of the World Medical Association (Declaration of Helsinki) and the standards established by the Institutional Review Board of the University of Pennsylvania and the National Institutes of Health. All subjects provided written informed consent for this study.

2.2. MRI acquisition and processing

MRI data used for this study was a part of multimodal MRI acquisition acquired on a 3-Tesla Siemens Trio MRI scanner. ASL data was acquired using pseudo-continuous labeling with a labeling time = 1.52 s, post labeling delay (PLD) = 1.5 s and labeling plane offset = 9 cm. 45 label-control pairs were acquired with a 2D echo planar imaging (EPI) readout with TR/TE = 4 s/18 ms, matrix size = 64×64, in plane resolution = $3.4 \times 3.4mm^2$, bandwidth = 3004 Hz/px, number of slices = 18, slice thickness = 6 mm with a 20% distance factor. T1-weighted image for each subject was acquired using a 3D magnetization-prepared rapid gradient echo (MPRAGE) protocol with TR/TE/TI = 1.9 s/2.89 ms/900 ms, flip angle = 9°, bandwidth = 170 Hz/px, voxel size = $1 \times 1 \times 1mm^3$, 176 slices, and was used for normalizing to the MNI152 template space.

Both MRI and PET data were processed using SPM12 (Penny et al., 2007), FSL (Jenkinson et al., 2012), Advanced Normalization Tools (ANTS) (Avants et al., 2011) and custom MATLAB scripts. ASL

processing included motion correcting the raw EPI time series (Wang, 2012). To compute absolute CBF (CBF in ml/100 g/min), a CBF time series was first obtained by pairwise control-label subtraction, normalizing by corresponding control image, and using a single compartment model with recommended parameters (Alsop et al., 2015) as follows:

$$CBF(\text{ml/100g/min}) = \frac{60 \times 100\lambda\Delta M e^{\omega/T_{1\,blood}}}{2\alpha T_{1\,blood} M_0 (1 - e^{-\tau/T_{1\,blood}})}$$

Here ΔM is the control label difference, $\lambda = 0.9$ ml/g is the blood-brain partition coefficient, $\omega = 1.5$ s is the PLD, $\tau = 1.52$ s is the labeling time, $\alpha = 0.85$ is the tagging efficiency, $T_{1,blood} = 1.65$ s is the T1 of blood, M_0 is the equilibrium magnetization of the brain, and is equal to the corresponding control image. A mean CBF map was obtained using a Structural Correlation with Robust Bayesian (SCRUB) estimation approach to remove artifacts from ASL-CBF images (Dolui et al., 2016a, 2016b). The method consisted of an explicit outlier removal stage based on a structural correlation criterion to remove egregious volumes (Dolui et al., 2016a) followed by voxelwise processing to remove local artifacts (Dolui et al., 2016b). The mean ASL data was coregistered to the T1 image using FSL boundary-based-registration. The T1 images were normalized to the MNI space using ANTs and the CBF maps were normalized to the MNI space by combining the ASL-T1 coregistration and ANTs normalization. Thereafter the CBF maps were partial volume corrected using the method by Johnson and colleagues (Johnson et al., 2005) assuming a ratio of 2.5 between gray matter and white matter perfusion. Relative CBF was computed by normalizing the CBF in each voxel by mean CBF in putamen, a gray matter region thought to be unaffected in early AD and, indeed, found to not differ between groups in the current analysis ($p > 0.05$, see results).

2.3. ^{18}F-FDG-PET acquisition and processing

^{18}F-FDG-PET/CT data from 31 controls and 49 MCI subjects were acquired on a Philips Gemini TF PET/CT scanner on the same day as that of MRI while that from 5 controls and 7 MCI subjects were acquired at an average of 18 (range: −13 to 106) and 15.3 (range: −6 to 97) days from the MRI acquisition. Subjects fasted for at least 4 h prior to their PET scan, and blood-glucose levels were below 180 mg/dl before an intravenous injection of 5.0 ± 0.5 mCi of ^{18}F-FDG while they rested with their eyes open. Approximately 30 min after the injection, a 30-minute 3D emission scan was obtained (six 5-minute frames, 256 mm FOV, 128×128 matrix, $2 \times 2 \times 2mm^3$ voxel size). The longer acquisition time was required to compensate for the reduced count of the low dose (5mCi) of the tracer used in the study than used in typical clinical scans. Line-of-response row-action maximum likelihood algorithm reconstruction using sharp setting was performed followed by CT attenuation correction.

The processing of the PET data involved coregistation to the high resolution T1 images using SPM12 with a normalized mutual correlation criterion. Thereafter the maps were normalized to the MNI space using ANTS as described for ASL-MRI. Standardized Uptake Value Ratio (SUVR) maps were generated by normalizing the raw counts with mean uptake in pons and cerebellar vermis (Landau et al., 2011) and were partial volume corrected similar to ASL.

2.4. Statistical analysis

For each analysis, age and sex covariates were removed from the voxel/region of interest (ROI) values by fitting a linear regression model to the data of the control subjects and thereafter applying the fitted model to both control and MCI groups. Note that this method was used to remove the effect of age and sex in the context of normal aging without confounding it with the relationship with disease. P values less than 0.05 were considered significant.

2.4.1. Voxel-wise group differences

At the voxel level, we assessed control-patient group differences with PET SUVR and ASL CBF using the nonparametric permutation-based randomise tool (Winkler et al., 2014) in FSL with the default value of 5000 permutations. The results were thresholded at $p < 0.05$ threshold-free cluster enhancement (TFCE) family-wise error (FWE) rate controlled. We performed visual comparison and also quantified the similarity in group-differences obtained with PET and ASL using Pearson's correlation between their T scores. Note that the raw T scores provide magnitudes of strength of the group differences without considering the significance levels. We also assessed control-MCI group difference with ^{18}F-FDG-PET by computing SUVR using putamen as the reference region similar to ASL.

2.4.2. ROI-based group differences

ROI analysis included posterior cingulate cortex (PCC) and hippocampus, which have previously been shown to demonstrate AD specific changes in ASL-MRI (Chen et al., 2011; Dolui et al., 2017; Xekardaki et al., 2015; Xie et al., 2019). The ROIs were extracted using the automated anatomical labeling (AAL) template (Tzourio-Mazoyer et al., 2002). We also used a composite meta-ROI constructed using the coordinates of the 5 most frequently cited regions (right and left angular gyri, bilateral posterior cingulate, and right and left inferior temporal gyri), previously shown sensitive to ^{18}F-FDG-PET hypometabolism in the AD continuum (Landau et al., 2011). Whole gray matter was used to assess global abnormalities and primary motor cortex was included as a control region. Mean CBF and SUVR between controls and MCI were compared using two sample T-tests.

2.4.3. ROC analyses for disease classification

The performance of each modality as a classifier to predict the disease status (control or MCI) was compared using area under the receiver operating characteristic curve (ROC AUC) obtained with logistic regression using Scikit-learn toolbox (Pedregosa et al., 2011). The ROC analysis was done with a stratified K-fold cross-validation. First, the original data was split into k stratified folds. Then the ROC analysis was done k rounds with the leave-one-out strategy and the mean ± standard deviations obtained from the k rounds for AUC, sensitivity and specificity have been reported to present more accurate estimate of the model prediction performance. ^{18}F-FDG SUVR, absolute and relative ASL-CBF in PCC ROI were used as the predictors given its a priori sensitivity to early AD (Chen et al., 2011; Dolui et al., 2017; Landau et al., 2011; Mosconi et al., 2009; Xekardaki et al., 2015). We also considered the mean SUVR in the meta-ROI defined above for FDG-PET.

3. Results

Data from 6 MCI and 1 control were excluded due to poor ASL data quality leaving 50 MCI and 35 controls for analysis. Demographics for this subsample are provided in Table 1.

3.1. Voxel-wise group differences

Fig. 1 shows the group averaged CBF (or FDG-SUVR) in the control and MCI subjects and their differences. The ASL scans showed reduced perfusion in the cerebellum indicating incomplete coverage or reduced signal in some subjects. The MCI group displayed significantly reduced SUVR in the bilateral and medial temporo-parietal regions, posterior cingulate cortex (PCC), inferior prefrontal cortex and also regions in the subcortical gray matter such as caudate and thalamus (Fig. 2A), consistent with the typically observed pattern of prodromal AD (Bailly et al., 2015; Chetelat et al., 2003; Landau et al., 2011; Mosconi et al., 2010). A similar pattern was also observed for absolute CBF measured using ASL-MRI (Fig 2B): the MCI group displayed significantly reduced CBF in medial and bilateral temporoparietal regions,

Table 1
Demographics of the cohort.

Demographics	Control	MCI
# Subjects (#Female)*	35 (20)	50 (16)
Age in years**	70.2 ± 6.9 (range: 56–83)	73.0 ± 7.0 years (range: 57–86)
Education in years (median (range))	18 (11)	17.5 (13)
MMSE (median (range))***	30 (5)	27 (6)

* Higher proportion of women in the control group ($\chi^2 = 5.33$, $p = 0.02$).
** Trend for older age in the MCI group ($T = 1.78$, $p = 0.08$).
*** Lower MMSE in MCI ($p < 0.0001$).

middle and posterior cingulate cortex, insula, the subcortical gray matter (caudate and thalamus) and the inferior frontal regions. Hypoperfusion assessed using relative CBF was more localized than the absolute CBF pattern (Fig 2C) and was most prominent in posterior cingulate cortex and medial parietal regions, although differences were also observed in the caudate and thalamus, medial and bilateral temporal lobe and inferior frontal lobe.

The ASL hypoperfusion patterns (both with absolute and relative CBF) without partial volume correction (PVC) was very similar to that with PVC, but the FDG-PET hypometabolism pattern without PVC was larger in extent and of higher significance particularly in the bilateral medial temporal lobe (hippocampus and amygdala) (see supplementary material). Notably cortical thickness was also significantly lower in the bilateral medial temporal lobe (supplementary material) and hence PVC reduced ^{18}F-FDG-PET group difference in this region.

To better visualize the overlap between MCI and control differences in ^{18}F-FDG SUVR and ASL-CBF, the statistical maps were overlaid in Fig. 3 (left subplot showing overlay with absolute CBF and right subplot showing relative CBF). Areas of greatest overlap for both absolute and relative CBF included the posterior cingulate/precuneus and medial and inferior temporal regions. While both modalities also displayed significant control-MCI differences in lateral temporal and parietal regions, they were proximal, but largely non-overlapping.

The Pearson's correlation coefficient between the T scores corresponding to the group-differences obtained with ^{18}F-FDG-PET SUVR and absolute ASL CBF was 0.46 ($p < 0.001$) while that between SUVR and relative CBF was 0.43 ($p < 0.001$). See the supplementary material for the scatter plots.

We also obtained control-MCI group differences with ^{18}F-FDG-PET data using putamen as a reference region to assess the same normalization region used for ASL, but the SUVR group difference was found to be markedly reduced and of lesser extent (data not shown) than that obtained using pons and cerebellar vermis. Note, pons and cerebellar vermis are not reliably acquired in 2D PCASL because of its inferior location (see Fig. 1), which is often susceptible to artifacts and hence was not used to compute relative CBF.

3.2. ROI-based group differences

The results of ROI analyses are shown in Fig. 4 (p values are FDR corrected). As expected, PCC ($p = 0.002$) and the meta-ROI ($p = 0.007$) displayed significant hypometabolism in MCI patients relative to controls. A trend of hypometabolism was also observed in the whole gray matter ($p = 0.054$). No significant differences were seen in a control region of primary motor cortices ($p = 0.94$). Hypometabolism was also not observed in hippocampus ($p = 0.30$) though the analysis without PVC showed strong hypometabolism in this region (see supplementary material). Absolute CBF also demonstrated significant reductions in AD-specific regions (PCC: $p < 0.001$, hippocampus: $p = 0.04$, meta-ROI: $p = 0.03$), in whole gray matter ($p = 0.02$), and also in the primary motor cortex ($p = 0.04$) relative to controls. Relative CBF showed significant hypoperfusion in PCC ($p < 0.001$) and
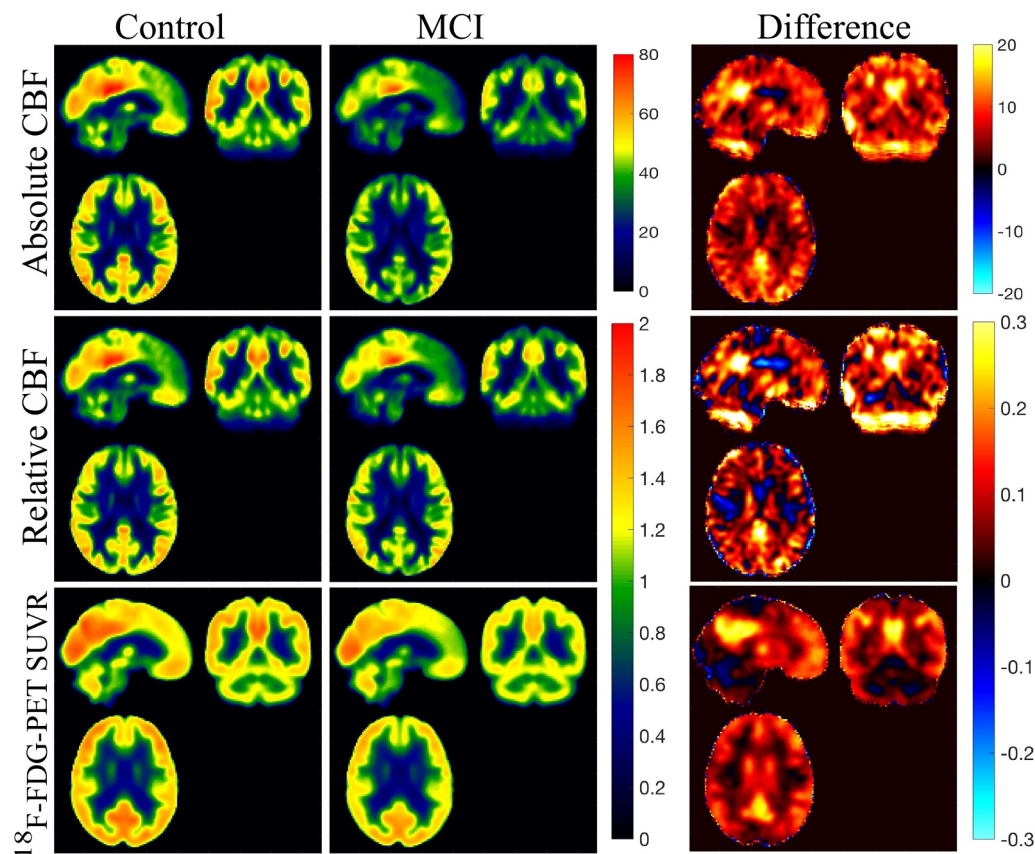
Fig. 1. Triaxial view of (left to right) average maps of the controls, MCI patients, and their differences for Absolute CBF (row 1), Relative CBF (row 2), and ^{18}F-FDG-PET SUVR (row 3).

whole gray matter (p = 0.005), a weak trend in the meta-ROI (p = 0.10), and no significant difference in hippocampus (p = 0.16) and M1 (p = 0.12). Note that absolute CBF in Putamen, which was used to obtain relative CBF, also did not differ between groups (mean CBF in controls: 54.82 ± 12.55, and in MCI = 51.88 ± 9.87 ml/100 g/min, p = 0.23).

3.3. ROC analysis for disease classification

The mean area under the receiver operating characteristic curve (ROC AUC) using 6-fold cross validation was calculated for each image type for performance comparison. Using the PCC ROI, all methods demonstrated moderate discriminatory power in predicting MCI status. ^{18}F-FDG SUVR, absolute CBF, and relative CBF had AUC (sensitivity, specificity) of 0.71 ± 0.12 (0.72 ± 0.15, 0.43 ± 0.24), 0.77 ± 0.12 (0.84 ± 0.12, 0.49 ± 0.23) and 0.74 ± 0.13 (0.74 ± 0.13, 0.61 ± 0.15), respectively. Absolute ASL CBF provided higher sensitivity, but lower specificity than relative CBF. The ROC curves are shown in Fig. 5. The AUC obtained with ^{18}F-FDG-PET in the meta-ROI was 0.71 ± 0.14 (0.74 ± 0.13, 0.44 ± 0.31). With the non-PVC SUVR, the corresponding results for PCC and the meta-ROI were 0.76 ± 0.13 (0.74 ± 0.17, 0.58 ± 0.27) and 0.75 ± 0.17 (0.76 ± 0.15, 0.53 ± 0.30) respectively.

4. Discussion

We compared ASL-MRI and ^{18}F-FDG-PET in 50 MCI patients and 35 matched controls to determine if ASL-MRI provides similar information about neurodegeneration to ^{18}F-FDG-PET. We demonstrated that (1) patterns of ASL-hypoperfusion overlapped with that of ^{18}F-FDG-PET-hypometabolism in MCI versus cognitively normal adults, particularly in midline parietal regions and (2) discrimination between these groups

is similar with both modalities using PCC-ROI commonly associated with prodromal AD abnormalities.

A general strength of this study is that ^{18}F-FDG-PET and ASL-MRI were obtained in close temporal proximity, usually on the same day. However, data from 12 subjects (7 MCI and 5 Controls) were not acquired on the same day, though acquired less than 4 months apart. A subgroup analysis with only the data obtained on the same day provided very similar effect sizes of the control-MCI group difference for both ASL and PET (data not shown).

Comparison of ASL and ^{18}F-FDG-PET was performed previously in late (Chen et al., 2011; Fallmar et al., 2017; Musiek et al., 2012; Verfaillie et al., 2015) and early (Verclytte et al., 2016) onset Alzheimer's disease, and demonstrated similar overlap of hypometabolism and hypoperfusion as described here. The current study population was MCI, a group likely enriched in prodromal AD, in whom differences with controls are expected to be subtler than in individuals with dementia. There have been a few prior studies that have examined MCI patients with ^{18}F-FDG-PET and ASL-MRI (Dolui et al., 2017; Riederer et al., 2018; Tosun et al., 2016). Specifically, in our prior study (Dolui et al., 2017), we focused on comparing different ASL modalities using FDG-PET as gold standard with a much smaller sample size. Riederer and colleagues (Riederer et al., 2018) used ASL with poorer pulsed labeling, which is characterized by weaker labeling than PCASL used in the current study and this might lead to their lack of difference in the ASL-MRI perfusion pattern between MCI and controls, unlike in this study. The study by Tosun and colleagues (Tosun et al., 2016) was also conducted using pulsed ASL data from the Alzheimer's Disease Neuroimaging Initiative (ADNI); further, the ASL and PET data were not acquired in close temporal proximity.

Examination of the spatial pattern of hypometabolism and hypoperfusion was broadly consistent across modalities and with the prior literature when comparing MCI/AD with cognitively normal adults
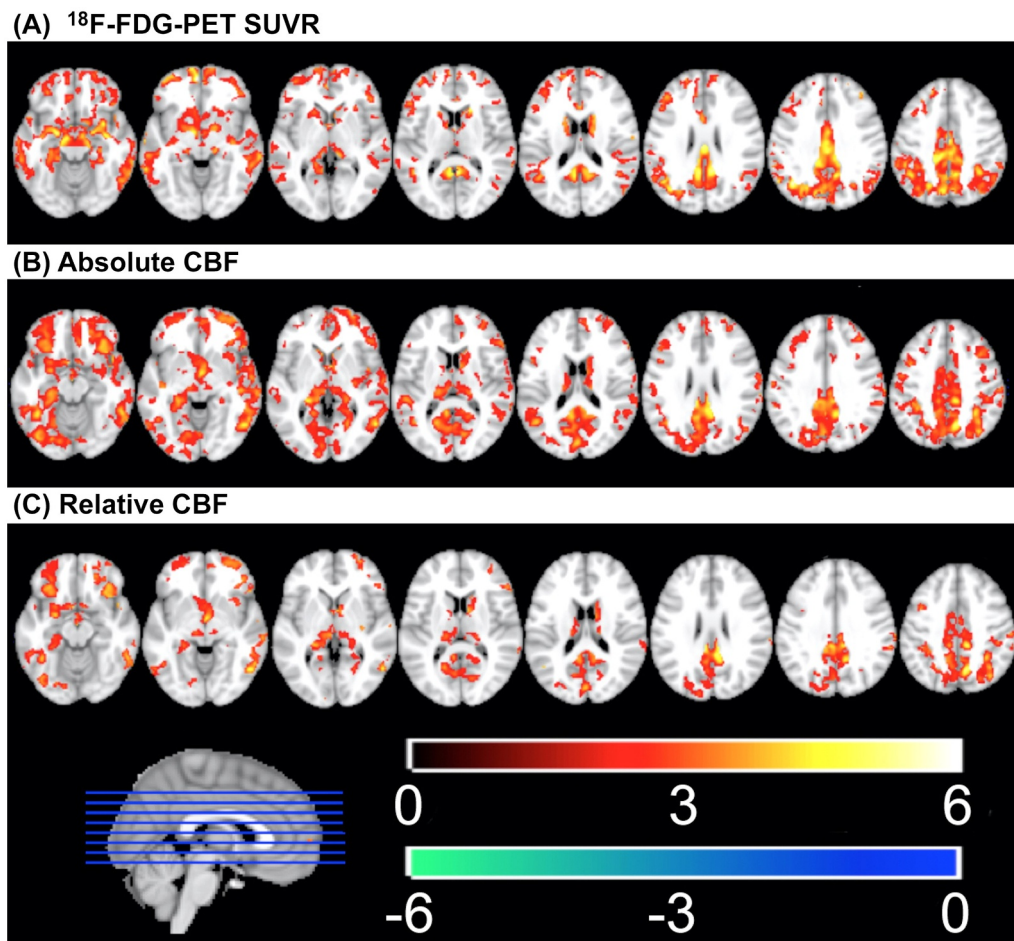
(A) ^{18}F-FDG-PET SUVR

(B) Absolute CBF

(C) Relative CBF

Fig. 2. Regions showing significant voxel level group differences between MCI and controls for A) ^{18}F-FDG-PET SUVR relative to uptake in pons and cerebellar vermis; B) absolute ASL-CBF; C) relative ASL-CBF relative to Putamen. Non-parametric two sample T tests were conducted with "randomise" tool of FSL toolbox, and the results were thresholded with $p < 0.05$ threshold-free cluster enhancement (TFCE) family-wise error (FWE) rate controlled. Hot color indicates lower in MCI than Control and cold color indicates higher in MCI than control.

(Dolui et al., 2017; Johnson et al., 2005; Landau et al., 2011; Mosconi et al., 2008; Riederer et al., 2018; Sierra-Marcos, 2017). The similarity in regional abnormalities in the MCI population was also evident from high correlation between the T-scores across all voxels. Interestingly, several regions in lateral cortical regions in parietal and temporal lobe had similar, but non-overlapping regions of significant

group differences. The basis for this discrepancy is uncertain, however blurring, geometric distortion, potential coregistration/normalization inaccuracies and difference in normalization regions may contribute. In addition, other non-AD pathological processes may be present in the heterogeneous construct of MCI, such as cerebrovascular disease, which might also differentially affect perfusion and metabolism and, thus,
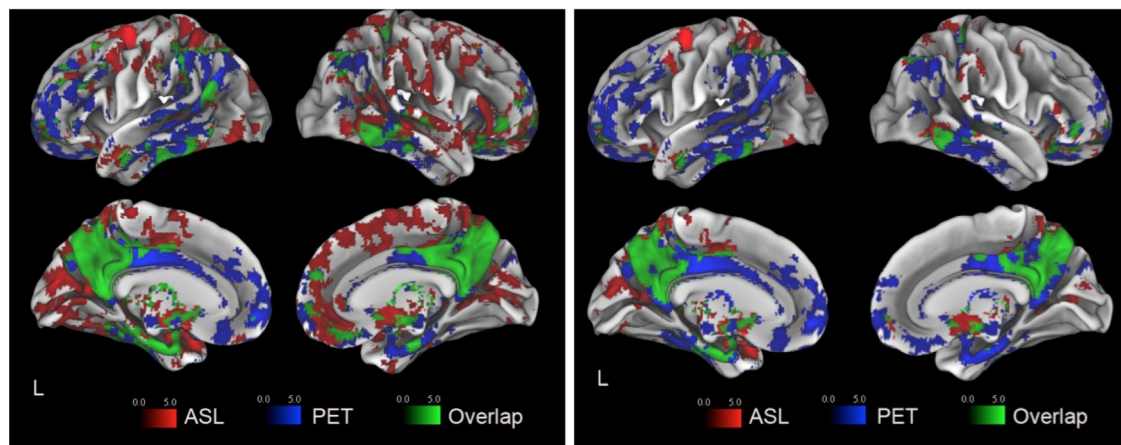

Fig. 3. Overlap of regions showing statistically significant group differences between MCI and control groups using ^{18}F-FDG-PET SUVR with Absolute (Left) and Relative CBF (Right); red indicates regions with group difference shown by ASL-CBF (absolute or relative), blue that with ^{18}F-FDG-PET SUVR and green showing the overlap of the two modalities. (For interpretation of the references to color in this figure legend, the reader is referred to the web version of this article.)
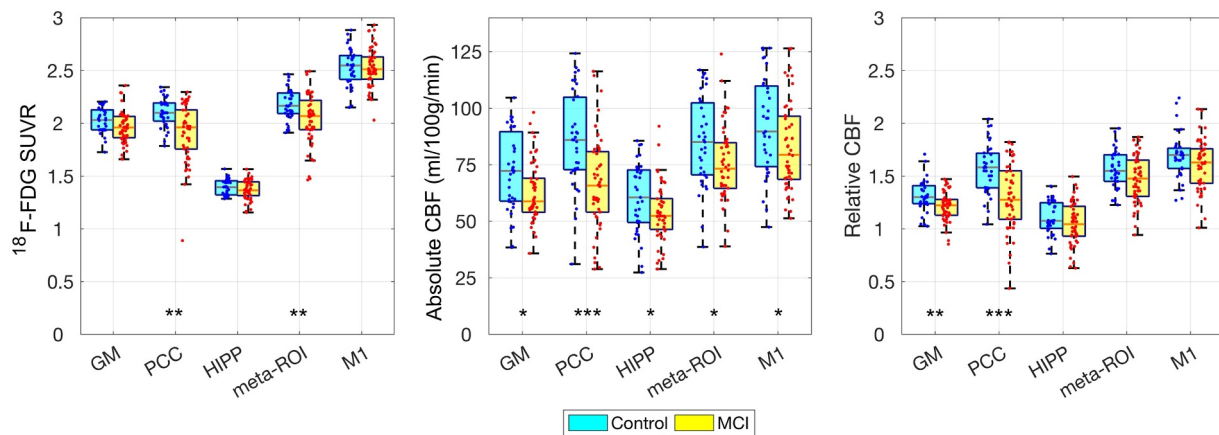
Fig. 4. Box plots with individual data points for group differences between MCI and normal controls in selected ROIs for (left) ^{18}F-FDG-PET SUVR relative to pons and cerebellar vermis uptake; (middle) absolute ASL-CBF; (right) relative ASL-CBF normalized to putamen. Abbreviations: GM: gray matter, PCC: posterior cingulate cortex; HIPP: hippocampus; meta-ROI: composite ROI sensitive to AD metabolic changes; M1: precentral cortex. Significant p values (FDR corrected) are marked with *: $p < 0.05$; **: $p < 0.01$; ***: $p < 0.001$.
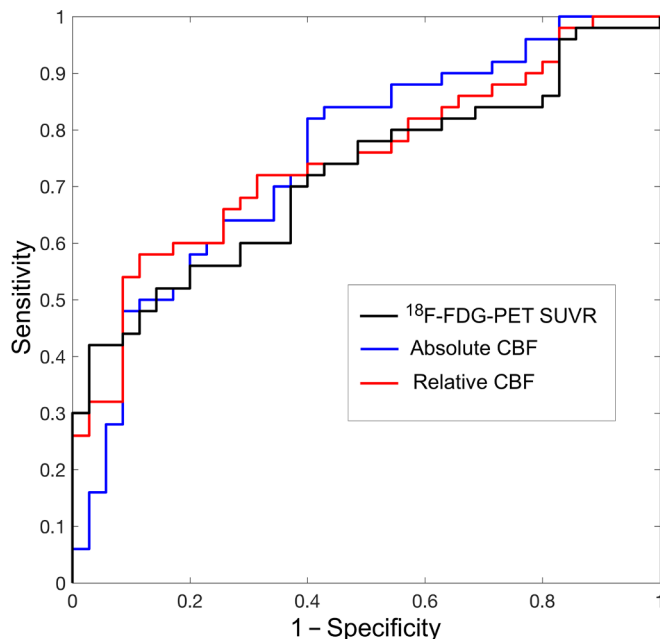

Fig. 5. Receiver Operating Characteristic (ROC) curves in classifying MCI patients and older controls using ^{18}F-FDG-PET SUVR, absolute and relative CBF.

cause the difference in the abnormality pattern measured by the two imaging modalities.

The PCC, which showed the strongest group difference in our study, has been consistently reported to be an early region of hypometabolism with ^{18}F-FDG-PET in the AD continuum (Drzezga et al., 2003; Herholz et al., 2002; Landau et al., 2012; Minoshima et al., 1997; Mosconi et al., 2009) and is perhaps the strongest and most consistent ROI in ASL-MRI studies of AD (Chen et al., 2011; Dai et al., 2009; Dolui et al., 2017; Johnson et al., 2005; Wolk and Detre, 2012; Xekardaki et al., 2015). Absolute CBF showed higher group difference and discriminatory power than relative CBF, but its global reduction in the diseased cohort and variability even in healthy population makes it relatively non-specific to AD. Relative CBF on the other hand reflected a more AD-specific pattern.

While one might expect partial volume correction (PVC) to have similar effects on both modalities, we found PVC to have less effect on ASL than on PET in that the control-MCI group difference in SUVR was

diminished after correction. Notably, from a clinical standpoint, the larger extent of SUVR reduction without PVC in diseased patients might make it easier to visually interpret the scans in neurodegenerative populations. However the AUC values obtained with non-PVC SUVR in a priori selected ROIs were similar to that of ASL.

The study has some limitations. First, the postlabeling delay (PLD = 1.5 s) for this study was shorter than the recently recommended values of 1.8–2 s (Alsop et al., 2015). However, we did not observe transit time artifacts in the mean CBF maps. Further, since the 2D acquisitions occurred slice by slice from the inferior to superior direction, the last slice was acquired 800 ms after the first slice leading to an average PLD of approximately 1.9 s across the brain, which is more comparable to the recommendations. Use of a 2D acquisition acquired without background suppression may also be considered a limitation relative to current "state-of-the-art" ASL, as increased sensitivity to AD using 3D background suppressed ASL was previously demonstrated (Dolui et al., 2017). Nonetheless, 2D acquisition is more widely available on MRI scanners, and this limitation was mitigated, in part, by the use of advanced signal processing strategies, although we had to discard data from 7 subjects due to poor ASL quality. It is also worth noting that because we did not have molecular measures of amyloid in a significant proportion of the cohort, we cannot comment on the specificity of the findings here to prodromal AD versus other causes of MCI. That said, this issue is equally present for ^{18}F-FDG-PET and the overlap between the two suggests that these modalities are likely to perform similarly with regard to specificity. Finally the study used a different reference region for ^{18}F-FDG-PET and ASL since we chose to use the optimal reference region for each method in this study.

In conclusion, ASL-MRI measurements of CBF produce considerable overlap with measures of ^{18}F-FDG-PET SUVR in known regions of early AD neurodegeneration. Given the possibility of adding ASL to routine structural MRI protocols without additional cost or exposure to ionization radiation, it may serve as a useful alternative to ^{18}F-FDG-PET for classifying the degree of neurodegeneration in individuals with prodromal AD especially in clinical research settings and also in clinical applications when FDG-PET is not available. While visual reads remain the gold standard in clinical practice, more automated, quantitative approaches such as used here do remain an important goal for the field. Future work should compare more advanced ASL-MRI methodologies with ^{18}F-FDG-PET in the same scanning session in longitudinal studies where their predictive value for disease progression can be evaluated. Effort should also be driven in comparing visual reads of individual scans to assess reliability of the ASL scans in clinical settings.

CRediT authorship contribution statement

Sudipto Dolui: Methodology, Software, Validation, Formal analysis, Writing - original draft, Funding acquisition. **Zhengjun Li:** Methodology, Software, Validation, Formal analysis, Writing - review & editing. **Ilya M. Nasrallah:** Methodology, Formal analysis, Writing - review & editing. **John A. Detre:** Conceptualization, Funding acquisition, Investigation, Writing - review & editing. **David A. Wolk:** Conceptualization, Funding acquisition, Investigation, Project administration, Writing - review & editing.

Declaration of Competing Interest

We believe there is no conflict of interest related to this work. However we disclose here that Dr. Wolk received personal fees for consultation from GE Healthcare, Merck, Eli Lilly, and Jannsen during the conduct of the study; and received grants from Avid Radiopharmaceuticals, Eli Lilly, Merck, Functional Neuromodulation, and Biogen outside the submitted work. Dr. Nasrallah received a grant from Avid Radiopharmaceuticals/Eli Lilly outside the submitted work.

Acknowledgements

Funding

Supplementary materials

Supplementary material associated with this article can be found, in the online version, at doi:10.1016/j.nicl.2019.102146.

References

Albert, M.S., DeKosky, S.T., Dickson, D., Dubois, B., Feldman, H.H., Fox, N.C., Gamst, A., Holtzman, D.M., Jagust, W.J., Petersen, R.C., Snyder, P.J., Carrillo, M.C., Thies, B., Phelps, C.H., 2011. The diagnosis of mild cognitive impairment due to alzheimer's disease: recommendations from the national institute on aging-alzheimer's association workgroups on diagnostic guidelines for Alzheimer's disease. Alzheimers Dement 7, 270–279.

Alsop, D.C., Detre, J.A., Golay, X., Gunther, M., Hendrikse, J., Hernandez-Garcia, L., Lu, H., Macintosh, B.J., Parkes, L.M., Smits, M., van Osch, M.J., Wang, D.J., Wong, E.C., Zaharchuk, G., 2015. Recommended implementation of arterial spin-labeled perfusion mri for clinical applications: a consensus of the ismrm perfusion study group and the european consortium for asl in dementia. Magn. Reson. Med. 73, 102–116.

Avants, B.B., Tustison, N.J., Song, G., Cook, P.A., Klein, A., Gee, J.C., 2011. A reproducible evaluation of ANTs similarity metric performance in brain image registration. Neuroimage 54, 2033–2044.

Bailly, M., Destrieux, C., Hommet, C., Mondon, K., Cottier, J.P., Beaufils, E., Vierron, E., Vercouillie, J., Ibazizene, M., Voisin, T., Payoux, P., Barre, L., Camus, V., Guilloteau, D., Ribeiro, M.J., 2015. Precuneus and cingulate cortex atrophy and hypometabolism in patients with alzheimer's disease and mild cognitive impairment: mri and (18)F-FDG pet quantitative analysis using freesurfer. Biomed. Res. Int. 2015, 583931.

Chen, Y., Wolk, D.A., Reddin, J.S., Korczykowski, M., Martinez, P.M., Musiek, E.S., Newberg, A.B., Julin, P., Arnold, S.E., Greenberg, J.H., Detre, J.A., 2011. Voxel-level comparison of arterial spin-labeled perfusion MRI and FDG-PET in Alzheimer disease. Neurology 77, 1977–1985.

Chetelat, G., Desgranges, B., de la Sayette, V., Viader, F., Eustache, F., Baron, J.C., 2003. Mild cognitive impairment: can FDG-PET predict who is to rapidly convert to Alzheimer's disease? Neurology 60, 1374–1377.

Dai, W., Lopez, O.L., Carmichael, O.T., Becker, J.T., Kuller, L.H., Gach, H.M., 2009. Mild cognitive impairment and alzheimer disease: patterns of altered cerebral blood flow at MR imaging. Radiology 250, 856–866.

Detre, J.A., Leigh, J.S., Williams, D.S., Koretsky, A.P., 1992. Perfusion imaging. Magn. Reson. Med. 23, 37–45.

Dolui, S., Vidorreta, M., Wang, Z., Nasrallah, I.M., Alavi, A., Wolk, D.A., Detre, J.A., 2017. Comparison of PASL, PCASL, and background-suppressed 3D pcasl in mild cognitive impairment. Hum. Brain Mapp. 38, 5260–5273.

Dolui, S., Wang, Z., Shinohara, R.T., Wolk, D.A., Detre, J.A., Alzheimer's Disease Neuroimaging, I., 2016. Structural correlation-based outlier rejection (SCORE) algorithm for arterial spin labeling time series. J. Magn. Reson. Imaging 45, 1786–1797.

Dolui, S., Wolk, D.A., Detre, J.A., 2016b. SCRUB: a structural correlation and empirical robust bayesian method for ASL data. In: Proceedings of the International Society of Magnetic Resonance in Medicine. Singapore.

Drzezga, A., Lautenschlager, N., Siebner, H., Riemenschneider, M., Willoch, F., Minoshima, S., Schwaiger, M., Kurz, A., 2003. Cerebral metabolic changes accompanying conversion of mild cognitive impairment into Alzheimer's disease: a PET follow-up study. Eur. J. Nucl. Med. Mol. Imaging 30, 1104–1113.

Ewing, J.R., Cao, Y., Knight, R.A., Fenstermacher, J.D., 2005. Arterial spin labeling: validity testing and comparison studies. J. Magn. Reson. Imaging 22, 737–740.

Fallmar, D., Haller, S., Lilja, J., Danfors, T., Kilander, L., Tolboom, N., Egger, K., Kellner, E., Croon, P.M., Verfaillie, S.C.J., van Berckel, B.N.M., Ossenkoppele, R., Barkhof, F., Larsson, E.M., 2017. Arterial spin labeling-based Z-maps have high specificity and positive predictive value for neurodegenerative dementia compared to FDG-PET. Eur. Radiol. 27, 4237–4246.

Heijtel, D.F., Mutsaerts, H.J., Bakker, E., Schober, P., Stevens, M.F., Petersen, E.T., van Berckel, B.N., Majoie, C.B., Booij, J., van Osch, M.J., Vanbavel, E., Boellaard, R., Lammertsma, A.A., Nederveen, A.J., 2014. Accuracy and precision of pseudo-continuous arterial spin labeling perfusion during baseline and hypercapnia: a head-to-head comparison with (1)(5)O H(2)O positron emission tomography. Neuroimage 92, 182–192.

Herholz, K., Salmon, E., Perani, D., Baron, J.C., Holthoff, V., Frolich, L., Schonknecht, P., Ito, K., Mielke, R., Kalbe, E., Zundorf, G., Delbeuck, X., Pelati, O., Anchisi, D., Fazio, F., Kerrouche, N., Desgranges, B., Eustache, F., Beuthien-Baumann, B., Menzel, C., Schroder, J., Kato, T., Arahata, Y., Henze, M., Heiss, W.D., 2002. Discrimination between alzheimer dementia and controls by automated analysis of multicenter FDG PET. Neuroimage 17, 302–316.

Herholz, K., Westwood, S., Haense, C., Dunn, G., 2011. Evaluation of a calibrated (18)F-FDG pet score as a biomarker for progression in Alzheimer disease and mild cognitive impairment. J. Nucl. Med. 52, 1218–1226.

Jack Jr., C.R., Bennett, D.A., Blennow, K., Carrillo, M.C., Dunn, B., Haeberlein, S.B., Holtzman, D.M., Jagust, W., Jessen, F., Karlawish, J., Liu, E., Molinuevo, J.L., Montine, T., Phelps, C., Rankin, K.P., Rowe, C.C., Scheltens, P., Siemers, E., Snyder, H.M., Sperling, R., Contributors, 2018. NIA-AA research framework: toward a biological definition of Alzheimer's disease. Alzheimers Dement 14, 535–562.

Jack Jr., C.R., Bennett, D.A., Blennow, K., Carrillo, M.C., Feldman, H.H., Frisoni, G.B., Hampel, H., Jagust, W.J., Johnson, K.A., Knopman, D.S., Petersen, R.C., Scheltens, P., Sperling, R.A., Dubois, B., 2016. A/T/N: an unbiased descriptive classification scheme for Alzheimer disease biomarkers. Neurology 87, 539–547.

Jack Jr., C.R., Knopman, D.S., Jagust, W.J., Petersen, R.C., Weiner, M.W., Aisen, P.S., Shaw, L.M., Vemuri, P., Wiste, H.J., Weigand, S.D., Lesnick, T.G., Pankratz, V.S., Donohue, M.C., Trojanowski, J.Q., 2013. Tracking pathophysiological processes in Alzheimer's disease: an updated hypothetical model of dynamic biomarkers. Lancet Neurol. 12, 207–216.

Jenkinson, M., Beckmann, C.F., Behrens, T.E., Woolrich, M.W., Smith, S.M., 2012. FSL. Neuroimage 62, 782–790.

Johnson, N.A., Jahng, G.H., Weiner, M.W., Miller, B.L., Chui, H.C., Jagust, W.J., Gorno-Tempini, M.L., Schuff, N., 2005. Pattern of cerebral hypoperfusion in Alzheimer disease and mild cognitive impairment measured with arterial spin-labeling MR imaging: initial experience. Radiology 234, 851–859.

Koziak, A.M., Winter, J., Lee, T.Y., Thompson, R.T., St Lawrence, K.S., 2008. Validation study of a pulsed arterial spin labeling technique by comparison to perfusion computed tomography. Magn. Reson. Imaging 26, 543–553.

Landau, S.M., Harvey, D., Madison, C.M., Koeppe, R.A., Reiman, E.M., Foster, N.L., Weiner, M.W., Jagust, W.J., Alzheimer's Disease Neuroimaging, I., 2011. Associations between cognitive, functional, and FDG-pet measures of decline in AD and MCI. Neurobiol. Aging 32, 1207–1218.

Landau, S.M., Harvey, D., Madison, C.M., Reiman, E.M., Foster, N.L., Aisen, P.S., Petersen, R.C., Shaw, L.M., Trojanowski, J.Q., Jack Jr., C.R., Weiner, M.W., Jagust, W.J., Alzheimer's Disease Neuroimaging, I., 2010. Comparing predictors of conversion and decline in mild cognitive impairment. Neurology 75, 230–238.

Landau, S.M., Mintun, M.A., Joshi, A.D., Koeppe, R.A., Petersen, R.C., Aisen, P.S., Weiner, M.W., Jagust, W.J., Alzheimer's Disease Neuroimaging, I., 2012. Amyloid deposition, hypometabolism, and longitudinal cognitive decline. Ann. Neurol. 72, 578–586.

Minoshima, S., Giordani, B., Berent, S., Frey, K.A., Foster, N.L., Kuhl, D.E., 1997. Metabolic reduction in the posterior cingulate cortex in very early Alzheimer's disease. Ann. Neurol. 42, 85–94.

Mosconi, L., Berti, V., Glodzik, L., Pupi, A., De Santi, S., de Leon, M.J., 2010. Pre-clinical detection of Alzheimer's disease using FDG-PET, with or without amyloid imaging. J. Alzheimers Dis 20, 843–854.

Mosconi, L., Mistur, R., Switalski, R., Tsui, W.H., Glodzik, L., Li, Y., Pirraglia, E., De Santi, S., Reisberg, B., Wisniewski, T., de Leon, M.J., 2009. FDG-PET changes in brain glucose metabolism from normal cognition to pathologically verified Alzheimer's disease. Eur. J. Nucl. Med. Mol. Imaging 36, 811–822.

Mosconi, L., Tsui, W.H., Herholz, K., Pupi, A., Drzezga, A., Lucignani, G., Reiman, E.M., Holthoff, V., Kalbe, E., Sorbi, S., Diehl-Schmid, J., Perneczky, R., Clerici, F., Caselli, R., Beuthien-Baumann, B., Kurz, A., Minoshima, S., de Leon, M.J., 2008. Multicenter standardized 18F-FDG PET diagnosis of mild cognitive impairment, Alzheimer's disease, and other dementias. J. Nucl. Med. 49, 390–398.

Musiek, E.S., Chen, Y., Korczykowski, M., Saboury, B., Martinez, P.M., Reddin, J.S., Alavi, A., Kimberg, D.Y., Wolk, D.A., Julin, P., Newberg, A.B., Arnold, S.E., Detre, J.A., 2012. Direct comparison of fluorodeoxyglucose positron emission tomography and arterial spin labeling magnetic resonance imaging in Alzheimer's disease. Alzheimers Dement. 8, 51–59.

Pedregosa, F., Varoquaux, G., Gramfort, A., Michel, V., Thirion, B., Grisel, O., Blondel, M., Prettenhofer, P., Weiss, R., Dubourg, V., 2011. Scikit-learn: machine learning in Python. J. Mach. Learn. Res. 12, 2825–2830.

Penny, W., Friston, K., Ashburner, J., Kiebel, S., Nichols, T.E., 2007. Statistical Parametric Mapping: The Analysis of Functional Brain Images. Academic Press.

Petersen, R.C., 2004. Mild cognitive impairment as a diagnostic entity. J. Intern. Med. 256, 183–194.

Raichle, M.E., 1998. Behind the scenes of functional brain imaging: a historical and physiological perspective. Proc. Natl. Acad. Sci. U S A 95, 765–772.

Riederer, I., Bohn, K.P., Preibisch, C., Wiedemann, E., Zimmer, C., Alexopoulos, P., Forster, S., 2018. Alzheimer disease and mild cognitive impairment: integrated pulsed arterial spin-labeling MRI and (18)F-FDG PET. Radiology 288, 198–206.

Selkoe, D.J., 2002. Alzheimer's disease is a synaptic failure. Science 298, 789–791.

Sierra-Marcos, A., 2017. Regional cerebral blood flow in mild cognitive impairment and alzheimer's disease measured with arterial spin labeling magnetic resonance imaging. Int. J. Alzheimers Dis. 2017, 5479597.

Tosun, D., Schuff, N., Jagust, W., Weiner, M.W., Alzheimer"s Disease Neuroimaging, I., 2016. Discriminative power of arterial spin labeling magnetic resonance imaging and 18F-Fluorodeoxyglucose positron emission tomography changes for amyloid-beta-positive subjects in the alzheimer's disease continuum. Neurodegener. Dis. 16, 87–94.

Tzourio-Mazoyer, N., Landeau, B., Papathanassiou, D., Crivello, F., Etard, O., Delcroix, N., Mazoyer, B., Joliot, M., 2002. Automated anatomical labeling of activations in spm using a macroscopic anatomical parcellation of the MNI MRI single-subject brain. Neuroimage 15, 273–289.

Verclytte, S., Lopes, R., Lenfant, P., Rollin, A., Semah, F., Leclerc, X., Pasquier, F., Delmaire, C., 2016. Cerebral hypoperfusion and hypometabolism detected by arterial spin labeling MRI and FDG-PET in early-onset Alzheimer's disease. J. Neuroimaging 26, 207–212.

Verfaillie, S.C., Adriaanse, S.M., Binnewijzend, M.A., Benedictus, M.R., Ossenkoppele, R., Wattjes, M.P., Pijnenburg, Y.A., van der Flier, W.M., Lammertsma, A.A., Kuijer, J.P., Boellaard, R., Scheltens, P., van Berckel, B.N., Barkhof, F., 2015. Cerebral perfusion and glucose metabolism in Alzheimer's disease and frontotemporal dementia: two sides of the same coin? Eur. Radiol. 25, 3050–3059.

Wang, Z., 2012. Improving cerebral blood flow quantification for arterial spin labeled perfusion MRI by removing residual motion artifacts and global signal fluctuations. Magn. Reson. Imaging 30, 1409–1415.

Warmuth, C., Nagel, S., Hegemann, O., Wlodarczyk, W., Ludemann, L., 2007. Accuracy of blood flow values determined by arterial spin labeling: a validation study in isolated porcine kidneys. J. Magn. Reson. Imaging 26, 353–358.

Winkler, A.M., Ridgway, G.R., Webster, M.A., Smith, S.M., Nichols, T.E., 2014. Permutation inference for the general linear model. Neuroimage 92, 381–397.

Wirth, M., Madison, C.M., Rabinovici, G.D., Oh, H., Landau, S.M., Jagust, W.J., 2013. Alzheimer's disease neurodegenerative biomarkers are associated with decreased cognitive function but not beta-amyloid in cognitively normal older individuals. J. Neurosci. 33, 5553–5563.

Wolk, D.A., Detre, J.A., 2012. Arterial spin labeling MRI: an emerging biomarker for Alzheimer's disease and other neurodegenerative conditions. Curr. Opin. Neurol. 25, 421–428.

Xekardaki, A., Rodriguez, C., Montandon, M.L., Toma, S., Tombeur, E., Herrmann, F.R., Zekry, D., Lovblad, K.O., Barkhof, F., Giannakopoulos, P., Haller, S., 2015. Arterial spin labeling may contribute to the prediction of cognitive deterioration in healthy elderly individuals. Radiology 274, 490–499.

Xie, L., Das, S.R., Pilania, A., Daffner, M., Stockbower, G.E., Dolui, S., Yushkevich, P.A., Detre, J.A., Wolk, D.A., 2019. Task-enhanced arterial spin labeled perfusion MRI predicts longitudinal neurodegeneration in mild cognitive impairment. Hippocampus 29, 26–36.

Xie, L., Dolui, S., Das, S.R., Stockbower, G.E., Daffner, M., Rao, H., Yushkevich, P.A., Detre, J.A., Wolk, D.A., 2016. A brain stress test: cerebral perfusion during memory encoding in mild cognitive impairment. Neuroimage Clin. 11, 388–397.

Ye, F.Q., Berman, K.F., Ellmore, T., Esposito, G., van Horn, J.D., Yang, Y., Duyn, J., Smith, A.M., Frank, J.A., Weinberger, D.R., McLaughlin, A.C., 2000. H(2)(15)O PET validation of steady-state arterial spin tagging cerebral blood flow measurements in humans. Magn. Reson. Med. 44, 450–456.